Electrodeposition of Nanopatterned Metal Oxides with Controlled Phase & Composition

Evan Carlson, Angel Burgos

June 14, 2024

Advisor: William Chueh
Industry Mentors: Tony Ricco, Cliff Knollenberg, Don Gardner
E241 Spring 2024

Contents

1 Introduction

1.1 Motivation

Electrodeposition is a powerful technique that enables deposition of a wide array of metals, metal oxides, and metal hydroxides with controlled phase and composition.[1-5] In contrast to physical vapor deposition, the ability to **selectively electrodeposit specific polymorphs of a material** is uniquely powerful, as the resulting structures can possess vastly different physical and chemical properties.[6] Despite these advantages, electrodeposition can be sensitive to slight variations in experimental conditions, including temperature, electrolyte composition, pH, current, voltage, etc. Perhaps due to these complexities, electrodeposition has been underutilized in nanofabrication.

In this work, we **combine electrodeposition with UV lithography to fabricate metal oxide nanopatterns of controlled composition and phase** on conductive substrates. While our primary motivation was to pattern battery and electrocatalyst materials (e.g. δ-MnO_2, α-$Ni(OH)_2$) into samples suitable for *operando* x-ray spectromicroscopy (STXM) (i.e. ~1-2 um wide and ~50-100 nm thick), the ability to control the phase and composition of nanopatterned metal oxides has wide applications. Although electrodeposition of pure metals into lithographic features has been previously explored,[7,8] published methods are limited and even less has been reported on deposition of metal (hydr)oxides. Moreover, as we show below, electrodeposition enables precise control over the height of deposited features.

1.2 Objectives

This work develops methods for electrodepositing metal (hydr)oxides into lithographically-defined features on conductive substrates, using δ-MnO_2, Mn_3O_4, and α-$Ni(OH)_2$ as example materials. It is then shown that electrodeposition parameters can be varied to control the surface uniformity and height of deposited features down to 100 nm.

1.3 Benefits to the SNF Community

The processes developed and demonstrated in this report are of use to researchers developing nanoscale devices in which metal (hydr)oxides play an important role in device functionality. For example, this includes controlled deposition of semiconductors, optical circuits, magnetic devices, and energy devices. Specifically, this work provides the SNF community with an SOP on the following:

1. Electrodeposition of materials with controlled phase and composition
2. Electrodeposition into lithographically-patterned features
3. Characterization of deposited features to measure height and surface uniformity

2 Experimental Methods and Results

2.1 Process Flow

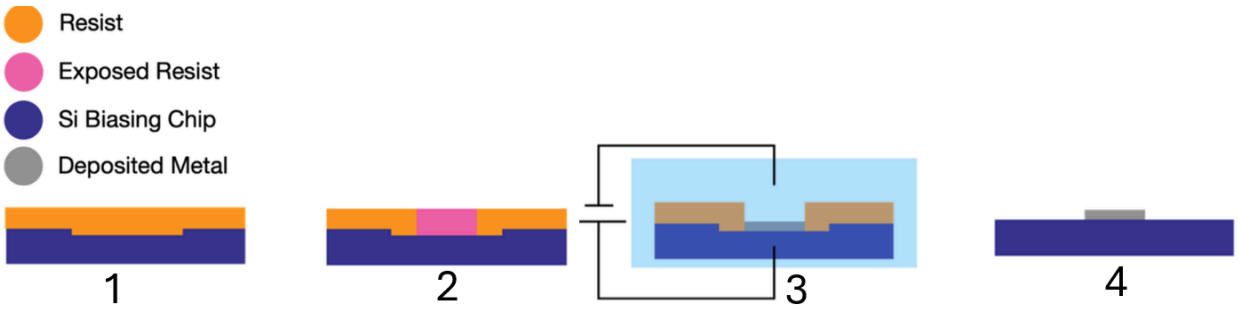

Figure 1: Schematic representation of procedure for electrodeposition of lithographic features.

A simplified schematic of the process for combining electrodeposition and lithography is depicted in Fig. 1. First, the conductive substrate is coated in photoresist (we used SPR 3612 resist on ITO-coated glass and Si chips with patterned glassy C electrodes). The photoresist is then exposed and developed to create a pattern of interest, followed by an optional descumming via O_2 plasma. The patterned substrate is then placed into a salt bath for electrodeposition. The process of electrodeposition is further depicted in Fig. 2.

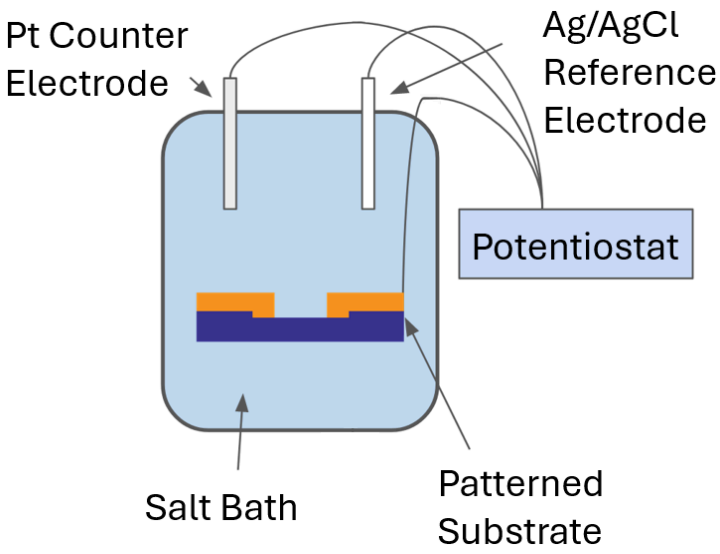

Figure 2: Schematic of electrodeposition setup.

As shown in Fig. 2, an electrodeposition setup consists of a reference electrode, counter electrode, salt bath, and voltage/current source. In this work, a leakless Ag/AgCl reference electrode (eDAQ) was used and a potentiostat (BioLogic SP-300) was used to control the applied voltage and/or current. The conductive sample is connected to the potentiostat as the working electrode. Although the connection is simplified in the schematic, it is important to note that the potentiostat leads should be kept outside of the salt bath while the exposed pattern is submerged. This prevents electrodeposition on unwanted surfaces, which would lead to inaccurate readings for current and total charge passed for deposition inside the pattern. After electrodeposition, the photoresist was removed by soaking the substrate in acetone.

As example materials, δ-MnO_2, Mn_3O_4, and α-$Ni(OH)_2$ were synthesized. δ-MnO_2 is a layered structure which can be used as a battery cathode material as well as an electrocatalyst for oxygen evolution and reduction.[2,9] Mn_3O_4 is a wide band semiconductor and can be used as a dielectric.[10] $Ni(OH)_2$ is used as an oxygen evolution catalyst.[11] Electrodeposition recipes were tested on ITO coated glass slides which were cleaned in acetone, isopropyl alcohol, and water before deposition. Cyclic voltammetry was used to find reaction peaks and was performed at a rate of 20 mV/s. All voltages are reported with respect to the Ag/AgCl reference electrode. Synthesized phases were characterized by Raman spectroscopy. Raman measurements (HORIBA LabRAM) were performed using a 532nm laser with 10% power, a dwell time of 10s, and averaged over 10 collections.

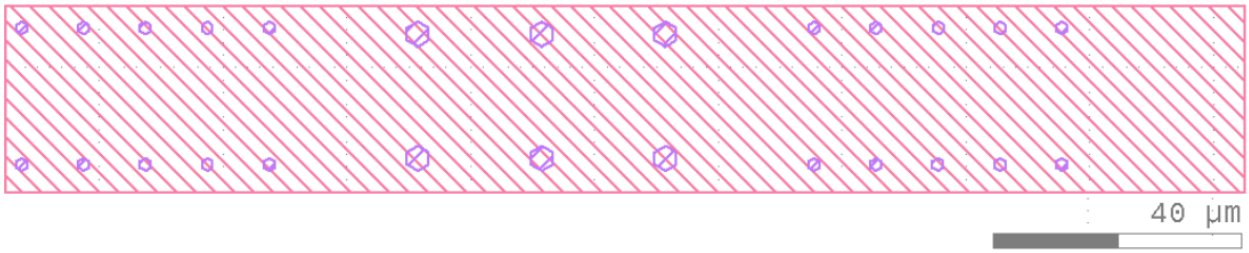

Figure 3: Lithography pattern used in this work.

The lithography pattern used in this work is shown in Fig. 3 and consists of two sizes of hexagons. Small hexagons have side lengths of 1 µm while larger hexagons have side lengths of 2 µm. Similar patterns were also used which contained a different number of features and sizes, but all patterns were within a 30 µm x 200 µm bounding box. It should be noted that this work utilized UV Lithography (Heidelberg 2), in which the limit is about 1 µm, leading to some features appearing rounded due to resolution. To measure the height and surface uniformity of deposited features, atomic force microscopy (AFM) was used.

2.2 Electrodeposition

2.21 δ-MnO_2

Electrodeposition of δ-MnO_2 was performed in a salt bath of 50mM KCl and 2mM $KMnO_4$ based on existing literature.[2] A cyclic voltammetry scan was performed between 0.8V and -0.5V, as shown in Fig. 4.

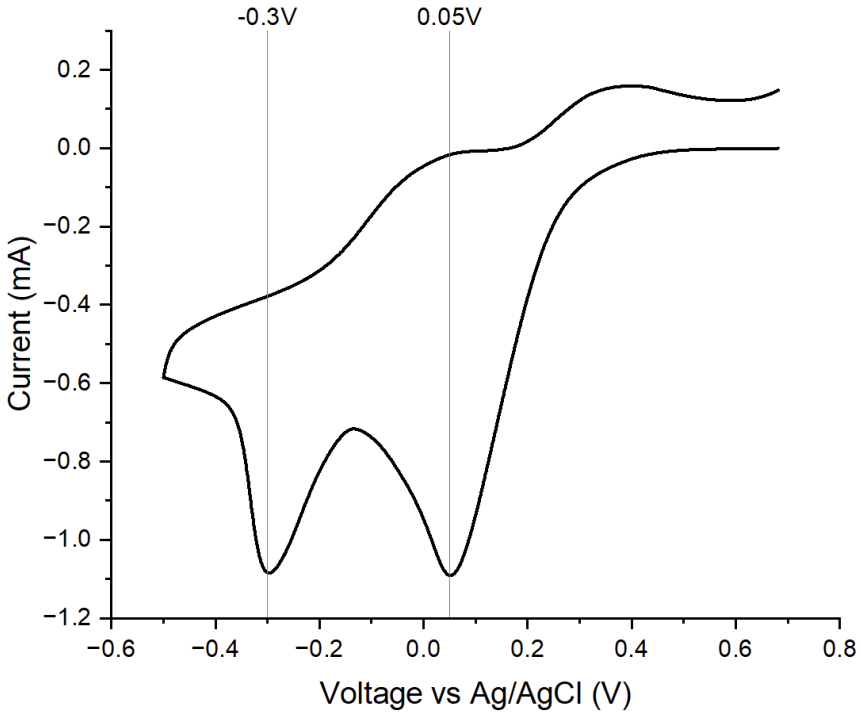

Figure 4: Cyclic voltammetry scan of $KMnO_4$ salt bath.

Substrate slides were placed in the salt bath and a potential of 0.05V was held for 10 minutes to deposit films thick enough for Raman spectroscopy measurements. Results are shown in Fig. 5 and demonstrate different deposited phases depending on if the salt bath was stirred during deposition. The spectrum of the unstirred sample closely matches reported data for δ-MnO_2.[12]

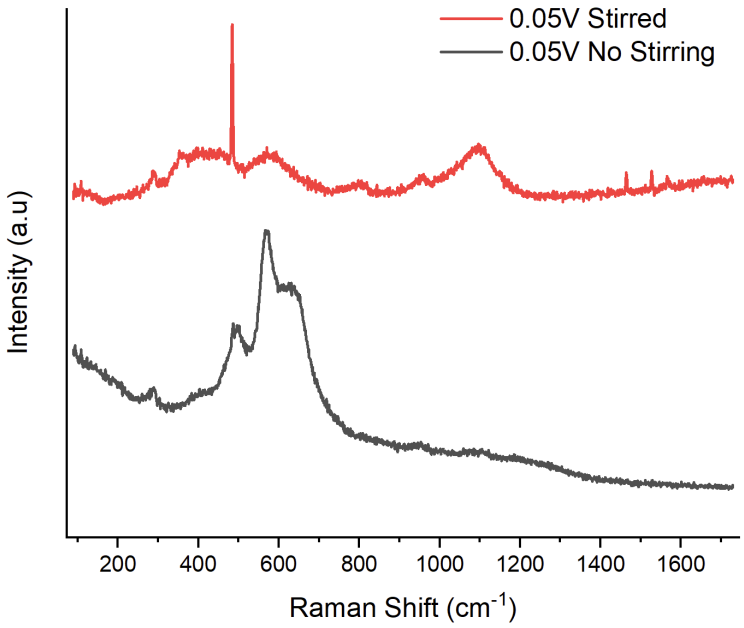

Figure 5: Raman spectra of $KMnO_4$ salt bath deposition at 0.05V with and without stirring.

2.22 Mn_3O_4

The same salt bath of 50mM KCl and 2mM $KMnO_4$ was used for Mn_3O_4 deposition. Samples were held at -0.3V vs Ag/AgCl for 10 minutes with stirring. The resulting raman spectrum shown in Fig. 6 matches reported data for Mn_3O_4.[13]

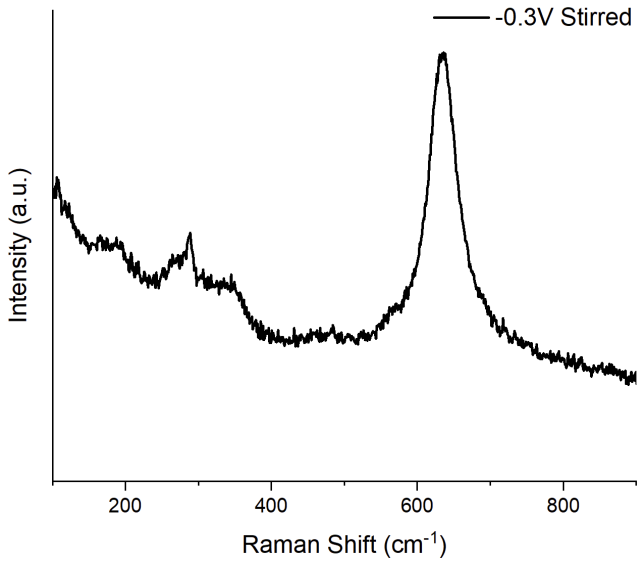

Figure 6: Raman spectrum of deposited Mn_3O_4.

2.23 α-$Ni(OH)_2$

Electrodeposition of α-$Ni(OH)_2$ was performed in a salt bath of 0.1M $Ni(NO_3)_2$. A cyclic voltammetry scan was performed between 0V and -1.5V and is shown in Fig. 7. While no obvious peaks were found outside of the increasing current due to hydrogen evolution at low voltages, it was noted that a white film developed on the substrate at around -1.22V on the oxidative sweep.

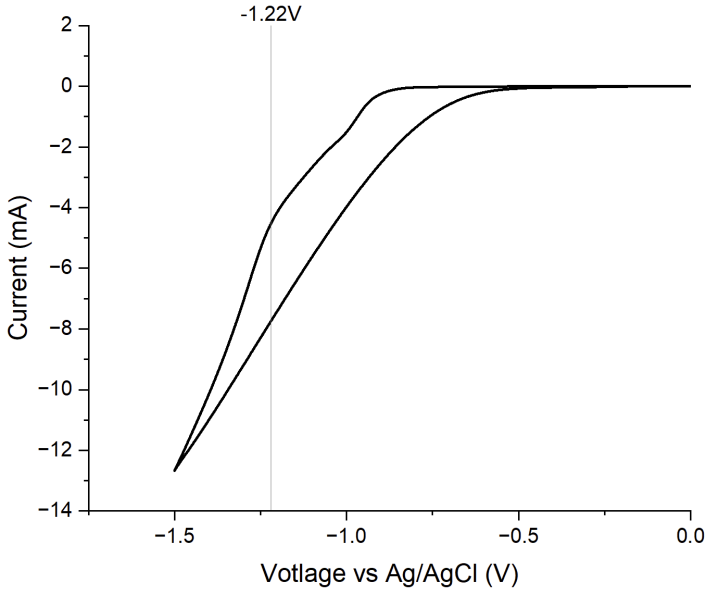

Figure 7: Cyclic voltammetry scan of $Ni(NO_3)_2$ salt bath.

A sample was held at -1.22V for 5 min to deposit a film. The resulting Raman spectrum is shown in Fig. 8 and matches reported data for α-$Ni(OH)_2$.[14]

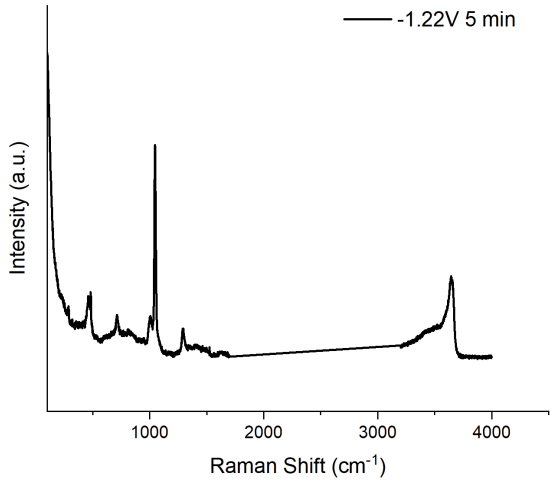

Figure 8: Raman spectrum of deposited α-$Ni(OH)_2$.

2.3 Electrodeposition in Lithographic Patterns

Electrodeposition inside lithographic patterns was done using the electrodeposition recipe developed for δ-MnO_2, while modifying deposition parameters that control the total charge passed to the substrate. To first test the uniformity of deposition, a 10 minute voltage hold was applied, resulting in the sample shown in Fig. 9. The dark features show scattered deposited features while most features remain unfilled.

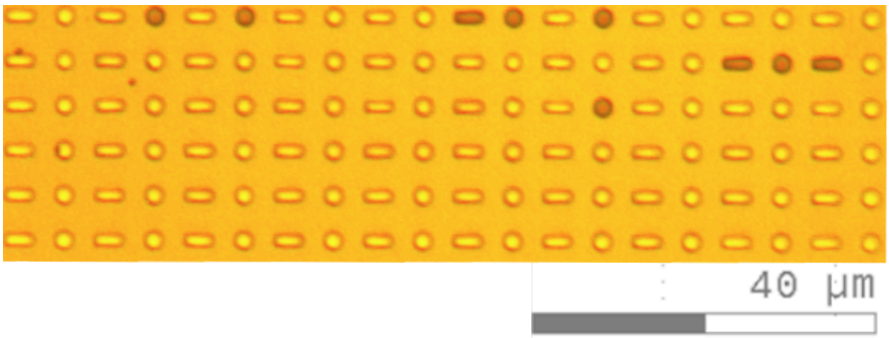

Figure 9: Pattern electrodeposition by 10 minute voltage hold.

To promote uniform deposition, a constant current of -1 µA was applied for 30s followed by a 15 second voltage hold at 0.05V. Total charge passed to the substrate was about 52 pC μm^{-2}. The resist was stripped and the deposited pattern is shown in Fig. 10. Feature heights were measured by atomic force, shown in Fig. 11, and showed even heights reaching about 850nm.

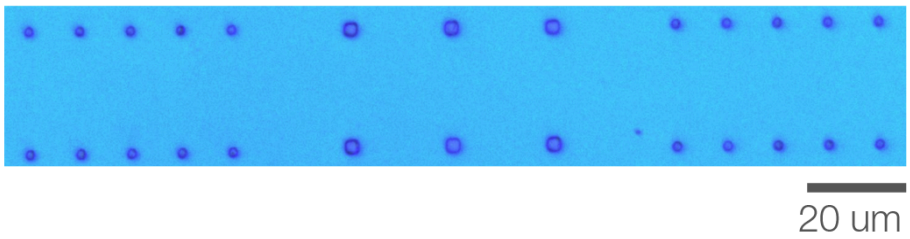

Figure 10: Pattern electrodeposition by constant current followed by voltage hold.

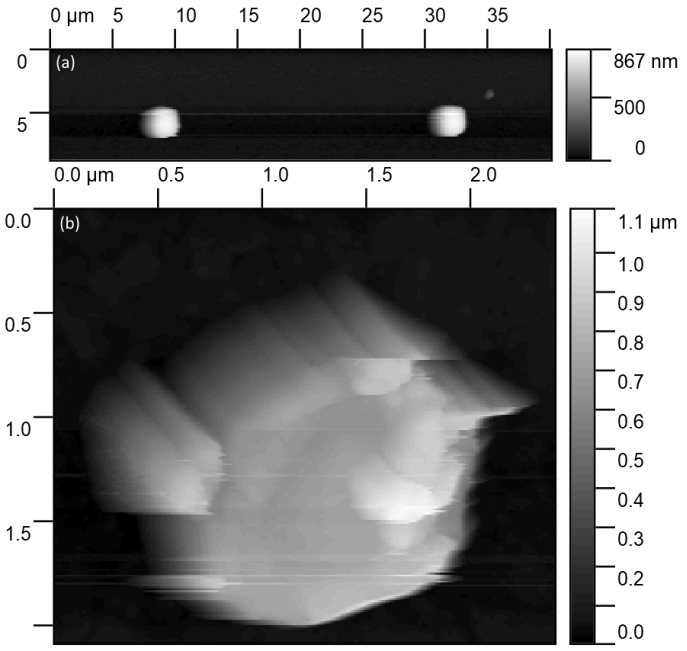

Figure 11: (a) AFM height map of features deposited by constant current and constant voltage. (b) Close up scan of feature. Note that smearing on the left edges of the particle is an artifact of these images being the AFM retrace of the height and indicative of a sudden drop in height.

To reduce the height of deposited samples further, a constant voltage approach was returned before combining constant current and constant voltage. While directly scaling total charge down by ⅛ would in theory result in a deposition height of about 100 nm, additional charge was added to account for other sources of current such as capacitive current unrelated to metal deposition. A constant voltage was then applied with a total charge cutoff of 13.1 pA μm^{-2}. The resulting features were 100 nm in height with ~1 nm of variation, as shown in Fig. 12.

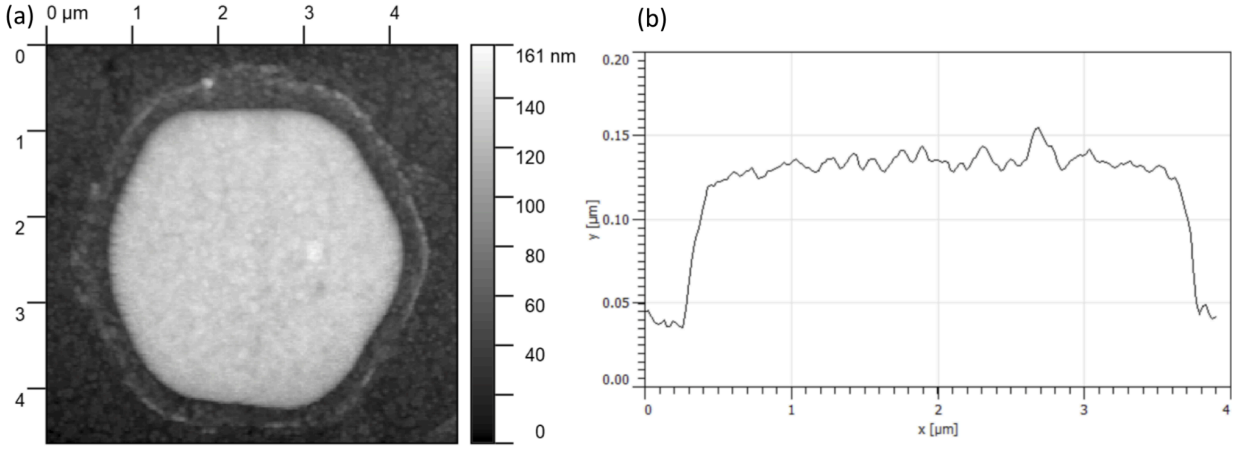

Figure 12: (a) AFM image height map of deposited feature after voltage hold with 13.1 pA μm^{-2} total charge cutoff. (b) Height map along the center horizontal line, showing 100 nm height from substrate to the top of the feature.

3 Discussion

3.1 Electrodeposition Phase Control

As shown in figures 4 and 7, cyclic voltammetry is a powerful tool for finding voltage windows of different reactions which can be used for electrodeposition in a given salt bath. Fig. 4 shows clear peaks from the $KMnO_4$ salt bath which can be attributed to the formation of δ-MnO_2 or Mn_3O_4. While Fig. 7 shows no distinct peaks for the $Ni(NO_3)_2$ salt bath, it can be noted that there is a slight shoulder around -1.22V. This is likely a reaction peak hidden by the large current induced by hydrogen evolution at the low voltage. Thus, it is important to note where the voltage window used is in relation to the hydrogen evolution reaction or the oxygen evolution reaction for a given aqueous salt bath.

The Raman spectra shown in Figures 5, 6, and 8 are in close agreement with spectra reported in the literature, signifying that the target phases were achieved. It is interesting to note that for the case of δ-MnO_2, stirring disrupted the formation of the desired phase. Previous reports have also shown that α-$Ni(OH)_2$ can be transformed into β-$Ni(OH)_2$ when exposed to strong alkaline solutions.[15] This highlights that beyond CV peaks, there are multiple methods of converting between polymorphs and compositions once a base layer has been electrodeposited.

3.2 Electrodeposition of Patterned Structures

Initial heterogeneous deposition shown in Fig. 9 is attributed to the competition between nucleation and growth. Once particles nucleate, it becomes lower energy for these particles to grow than for other features to become nucleated as well. Similarly, it may also be lower energy for larger particles to grow than smaller particles, thus larger particles may grow first. For this reason, it is proposed that applying constant current serves to nucleate the features evenly which can then be further grown by applying a constant voltage.

The heightmap in Fig. 11 shows the feature is composed of multiple large particles leading to an uneven surface. While this issue was not seen when the total height was reduced, it can be noted that multiple methods can be utilized to reduce the particle size and enhance surface uniformity. This includes pulsing the applied voltage or current repetitively for short periods to invoke rapid small scale deposition followed by relaxation. For methods where constant current is applied, it is also useful to note that applying a smaller current over a longer period of time typically results in smaller particles and improved uniformity.

Finally, the relationship between total charge passed and achieved height shown in Figures 11 and 12 demonstrate that not all charge is utilized for the deposition reaction. This leads to an empirical approach when developing calibration curves between deposited height and total charge passed. While not discussed in this work, the deposition parameters outside of total charge will also have an impact on the morphology of the deposited material, which may be another aspect of electrodeposition which can be controlled.

3.3 Future Work

As this work utilized UV lithography, the resolution limit for patterns to be tested was on the order of 1 μm. Future works can be aimed at developing electrodeposition techniques at smaller scales using e-beam lithography. Another useful goal is to develop calibration curves to determine the total charge passed necessary for a given electrodeposition recipe. Finally, as there are a vast number of materials that can be synthesized by electrodeposition, it will be important to explore different systems which require deposition methods other than constant voltages or require additional processing steps such as annealing.

4 Conclusions

Electrodeposition is a powerful and versatile technique which has been demonstrated to be applicable to lithographic patterns in this work. Cyclic voltammetry is shown to result in distinguishable peaks corresponding to electrochemical reactions which can be used to create synthesis procedures for various target phases. These phases can then be characterized by methods such as Raman spectroscopy, which can then be compared to reported data in literature. Finally, it has been demonstrated that electrodeposition parameters can be tuned to create features with controlled height down to 100 nm and a uniform surface. As such, electrodeposition serves as a powerful alternative to other deposition techniques for depositing material with controlled phases and morphologies for use in micro- and nano-scale devices.

5 Acknowledgements

The authors would like to give a special thanks to Swaroop, Tony, Cliff, and Don for guidance and suggestions throughout this work.

6 Budget

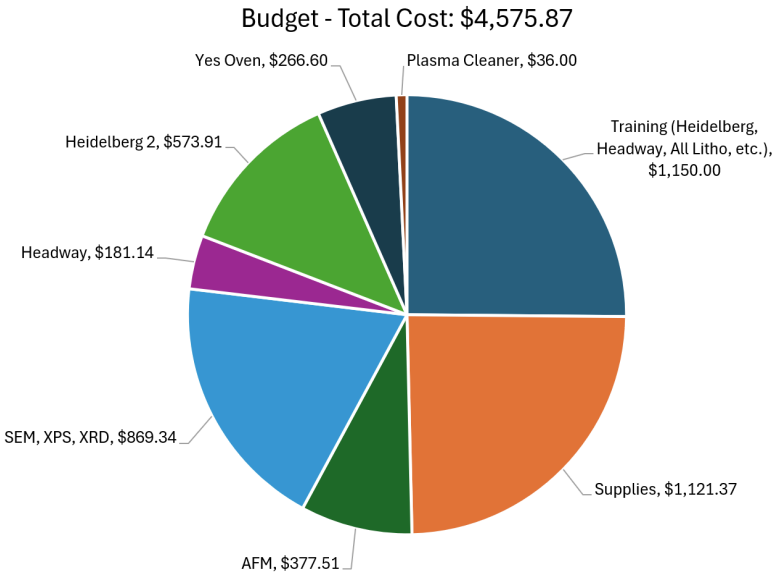

7 References

1. Yan, Z.; Liu, H.; Hao, Z.; Yu, M.; Chen, X.; Chen, J. Electrodeposition of (Hydro)Oxides for an Oxygen Evolution Electrode. Chem. Sci. 2020, 11 (39), 10614–10625. https://doi.org/10.1039/D0SC01532F.
2. Risch, M.; Stoerzinger, K. A.; Han, B.; Regier, T. Z.; Peak, D.; Sayed, S. Y.; Wei, C.; Xu, Z.; Shao-Horn, Y. Redox Processes of Manganese Oxide in Catalyzing Oxygen Evolution and Reduction: An in Situ Soft X-Ray Absorption Spectroscopy Study. J. Phys. Chem. C 2017, 121 (33), 17682–17692. https://doi.org/10.1021/acs.jpcc.7b05592.
3. Batchellor, A. S.; Boettcher, S. W. Pulse-Electrodeposited Ni–Fe (Oxy)Hydroxide Oxygen Evolution Electrocatalysts with High Geometric and Intrinsic Activities at Large Mass Loadings. ACS Catal. 2015, 5 (11), 6680–6689. https://doi.org/10.1021/acscatal.5b01551.
4. Burke, M. S.; Kast, M. G.; Trotochaud, L.; Smith, A. M.; Boettcher, S. W. Cobalt–Iron (Oxy)Hydroxide Oxygen Evolution Electrocatalysts: The Role of Structure and Composition on Activity, Stability, and Mechanism. J. Am. Chem. Soc. 2015, 137 (10), 3638–3648. https://doi.org/10.1021/jacs.5b00281.
5. Moulai, F.; Cherchour, N.; Messaoudi, B.; Zerroual, L. Electrosynthesis and Characterization of Nanostructured MnO2 Deposited on Stainless Steel Electrode: A Comparative Study with Commercial EMD. Ionics 2017, 23 (2), 453–460. https://doi.org/10.1007/s11581-016-1842-7.

6. Saha, B. K.; Nath, N. K.; Thakuria, R. Polymorphs with Remarkably Distinct Physical and/or Chemical Properties. The Chemical Record 2023, 23 (1), e202200173. https://doi.org/10.1002/tcr.202200173.
7. Jung, W.; Jang, S.; Cho, S.; Jeon, H.; Jung, H. Recent Progress in Simple and Cost‐Effective Top‐Down Lithography for ≈10 Nm Scale Nanopatterns: From Edge Lithography to Secondary Sputtering Lithography. Advanced Materials 2020, 32 (35), 1907101. https://doi.org/10.1002/adma.201907101.
8. Ahn, J.; Hong, S.; Shim, Y.-S.; Park, J. Electroplated Functional Materials with 3D Nanostructures Defined by Advanced Optical Lithography and Their Emerging Applications. Applied Sciences 2020, 10 (24), 8780. https://doi.org/10.3390/app10248780.
9. Wang, D.; Wang, L.; Liang, G.; Li, H.; Liu, Z.; Tang, Z.; Liang, J.; Zhi, C. A Superior δ-MnO 2 Cathode and a Self-Healing Zn-δ-MnO 2 Battery. ACS Nano 2019, 13 (9), 10643–10652. https://doi.org/10.1021/acsnano.9b04916.
10. Abdullah, M. M.; Siddiqui, S. A.; Al-Abbas, S. M. Physio-Chemical Properties and Dielectric Behavior of As-Grown Manganese Oxide (γ-Mn2O3) Nanoparticles. J. Electron. Mater. 2020, 49 (7), 4410–4417. https://doi.org/10.1007/s11664-020-08171-1.
11. Klaus, S.; Cai, Y.; Louie, M. W.; Trotochaud, L.; Bell, A. T. Effects of Fe Electrolyte Impurities on Ni(OH) 2 /NiOOH Structure and Oxygen Evolution Activity. J. Phys. Chem. C 2015, 119 (13), 7243–7254. https://doi.org/10.1021/acs.jpcc.5b00105.
12. Zhang, J.; Li, Y.; Wang, L.; Zhang, C.; He, H. Catalytic Oxidation of Formaldehyde over Manganese Oxides with Different Crystal Structures. Catal. Sci. Technol. 2015, 5 (4), 2305–2313. https://doi.org/10.1039/C4CY01461H.
13. Mahamad Yusoff, N. F.; Idris, N. H.; Md Din, M. F.; Majid, S. R.; Harun, N. A.; Rahman, M. M. Electrochemical Sodiation/Desodiation into Mn 3 O 4 Nanoparticles. ACS Omega 2020, 5 (45), 29158–29167. https://doi.org/10.1021/acsomega.0c03888.
14. Hall, D. S.; Lockwood, D. J.; Bock, C.; MacDougall, B. R. Nickel Hydroxides and Related Materials: A Review of Their Structures, Synthesis and Properties. Proc. R. Soc. A. 2015, 471 (2174), 20140792. https://doi.org/10.1098/rspa.2014.0792.
15. Zhang, J.; Zhang, T.; Feng, S. α-Ni(OH)2 Electrodeposition from NiCl2 Solution. Transactions of Nonferrous Metals Society of China 2020, 30 (10), 2802–2811. https://doi.org/10.1016/S1003-6326(20)65422-X.